

Ar-ion bombardment effects on ZrO₂ surfaces

C. Morant, J. M. Sanz, and L. Galán

Departamento Física Aplicada C-XII, Universidad Autónoma Madrid, Cantoblanco, E-28049 Madrid, Spain

(Received 13 June 1991)

Chemical, compositional, and electronic changes induced by 3-keV Ar⁺ sputtering in ZrO₂ have been quantitatively studied by use of x-ray photoemission spectroscopy. It is shown that 3-keV Ar⁺ bombardment leads to a gradual buildup of an oxygen depletion layer which has been quantitatively characterized by its thickness (~1.2 nm), averaged composition (~ZrO), and in-depth distribution of the different oxide phases that originate during the process. In addition, the electronic distribution at the valence band of both thermally grown and Ar⁺-bombarded ZrO₂ was also determined by x-ray photoemission spectroscopy. Thermally grown ZrO₂ was shown to exhibit significant photoemission in the band gap, probably due to defects. Ar⁺ bombardment of those surfaces caused a broadband emission at 2.3 eV above the top of the valence band as well as significant changes in the O 2*p* region of the valence band which are associated with the above-mentioned changes in surface composition. The Zr 4*d* contribution to the valence band of the altered layer could also be estimated. This contribution increases with Ar⁺ sputtering and accounts not only for the whole emission band in the gap but also significantly for the photoemission in the O 2*p* energy range.

I. INTRODUCTION

It is well known that ion bombardment of solids causes a wide series of both compositional and structural changes which influence their properties.^{1,2} However, quantitative studies relating compositional changes and modifications of the electronic structure induced by ion bombardment are very scarce.

In the case of transition-metal oxides, the study of their reduction to lower oxidation states (even to metal) and the creation of point defects by low-energy ion bombardment have been separate subjects of many recent studies.²⁻¹² In fact, although the surface properties of partially reduced oxides are important from both fundamental and technological points of view because of their chemisorptive and catalytic properties,¹³ fundamental questions regarding the electronic structure still remain, and constitute an interesting and actual discussion topic.^{7,9-11,13}

In the particular case of ZrO₂ its broad use for nuclear and high-temperature applications also makes that information about the effects of low-energy ion radiation of great interest. In spite of that, quantitative studies on the Ar⁺-induced reduction of ZrO₂ are very scarce.^{8,14,15}

In the present work the 3-keV-Ar⁺-induced chemical and electronic effects on thermally and anodically grown ZrO₂ films have been quantitatively characterized. The chemical state of Zr in Ar⁺-bombarded ZrO₂ has been examined in detail as a function of the Ar⁺ fluence using core-level x-ray photoemission spectroscopy (XPS). In addition, measurements at two different takeoff angles allowed one to obtain useful information about the distribution in depth of the different species observed as well as about the structure and the formation of the altered layer. We present a quantitative analysis of the buildup and structure of the altered layer induced in ZrO₂ by 3-keV Ar⁺ bombardment. In this case the photoelectron escape

depths resulted in being quite appropriate for probing the altered layer.

Valence-band spectra of the Ar⁺-modified surfaces were also taken in order to observe the effect in the electronic distribution at the valence band. In spite of having less sensitivity and resolution than ultraviolet photoemission spectroscopy (UPS), the use of XPS to obtain the valence band allowed one to get a straightforward and quantitative correlation between the modifications in the electron structure and the compositional changes.

II. EXPERIMENTAL

Polycrystalline zirconium sheets (25 μm thick) from Goodfellow Metals (99.7% nominal purity) and 10×18 mm² area were used in this work. They were subjected to the usual cleaning procedures, by rinsing the samples subsequently in acetone, ethanol, and distilled water before the thermal or anodic ZrO₂ was grown.

Thermally grown ZrO₂ was obtained by annealing the foil at 525 K, for 15 min in an oxygen atmosphere ($P_{O_2} \approx 10^{-5}$ Torr) in a preparation chamber attached to the spectrometer.

Anodic ZrO₂ layers (~50 nm thick) were obtained by anodizing the Zr foil in an 0.3 wt % aqueous solution of PO₄H₃ at room temperature with constant current density (0.23 mA/cm²) until a final voltage of 15 V was reached.

Ar⁺ bombardment was performed in the spectrometer chamber using an ion gun working at 3 keV and a current density of 1.5 μA/cm². The ion beam was rastered over the whole sample in order to avoid crater effects which could influence the quantification. Under those conditions the estimated sputter rate for standard Ta₂O₅ was ~0.01 nm s⁻¹.

XPS spectra were recorded at different intervals of ion bombardment in a commercial LHS-10 spectrometer

from Leybold using Mg $K\alpha_{1,2}$ radiation ($h\nu=1253.6$ eV) as excitation source. The electron energy analyzer was operated in the constant pass energy mode ($E_{\text{pass}}=20$ eV) with an energy resolution of 0.25 eV. Photoelectrons were usually collected normal to the sample but in some cases spectra at 30° with respect to the surface normal were also measured in order to enhance the surface sensitivity.

III. RESULTS AND DISCUSSION

A. Core-level spectra

Figure 1 shows experimental Zr $3d$ and O $1s$ XPS spectra of a thermally grown ZrO_2 sample as a function of the 3-keV Ar^+ fluence (indicated with each spectrum). The overall effect of the Ar^+ bombardment may be clearly observed in that figure. The Zr $3d$ spectrum, characteristic of ZrO_2 ,¹⁶ undergoes significant broadening with the appearance of a broad tail at the low-energy side of the spectrum, while the O $1s$ line reduces its intensity. All that clearly suggests that Ar^+ bombardment of ZrO_2 results in loss of oxygen at the surface and formation of Zr species in lower oxidation states.

In order to get a more quantitative insight on the Ar^+ -induced compositional changes and the buildup of the altered layer, the spectra were numerically processed and quantitatively analyzed. The spectra were smoothed^{17,18} and background subtracted^{19,20} according to the usual procedures. Then, the Zr $3d$ spectra were analyzed in terms of five possible valence states of Zr (i.e., Zr^{4+} , Zr^{3+} , Zr^{2+} , Zr^+ , and Zr^0) which would correspond to ZrO_2 , Zr_2O_3 , ZrO , Zr_2O , and metallic Zr, respectively, in accordance with a previous study on the room-temperature oxidation of zirconium.¹⁶ The line shape and fitting parameters of the different components have been summarized in Table I, whereas the detailed description of the analysis and fitting procedure is given in Ref. 16. The O $1s$ spectra were analyzed in terms of two components, the main peak at $E_b=531.4$ eV and a

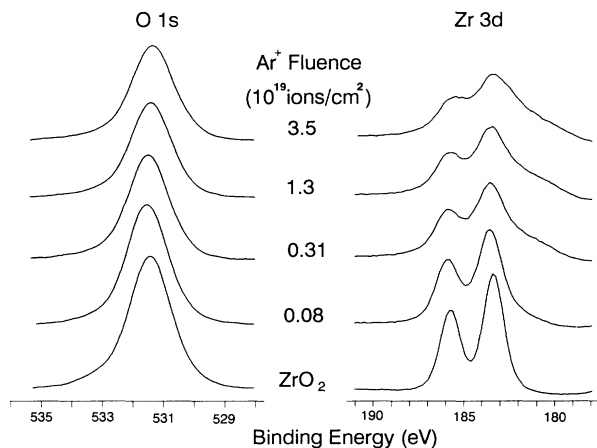


FIG. 1. XPS spectra of the Zr $3d$ and O $1s$ lines of ZrO_2 after different Ar^+ fluences.

TABLE I. Best-fit parameters for Zr $3d$ XPS spectra. Energies are in eV.

| Parameter | Value |
|---|--------|
| Binding energy of oxide $\text{Zr}^{4+} 3d_{5/2}$ | 183.40 |
| Metal-oxide chemical shift | 4.4 |
| Spin-orbit splitting | 2.39 |
| Shape and width of oxide peaks: | |
| Gaussian ^a FWHM | 1.4 |
| Lorentzian ^a FWHM | 0.7 |
| Total FWHM | 1.88 |

^aThe Mg $K\alpha$ line shape has been considered in the deconvolution.

small contribution at $E_b=533.6$ eV which were assigned to oxygen in an oxide state (i.e., O_{ox}) and to adsorbed oxygen (i.e., O_{ad}),¹⁶ respectively.

The intensities of the different components have been depicted in Fig. 2 as a function of the Ar^+ fluence. Figure 2(a) presents the behavior of the different oxidation states of zirconium. It clearly shows that Ar^+ bombardment causes a progressive decrease of the Zr^{4+} species and the continuous formation of species with lower oxidation states until a steady state is reached at fluences above 1.5×10^{19} ions/cm². In fact, the progressive loss of oxygen which causes that reduction of the Zr^{4+} species can also be followed by observing the corresponding in-

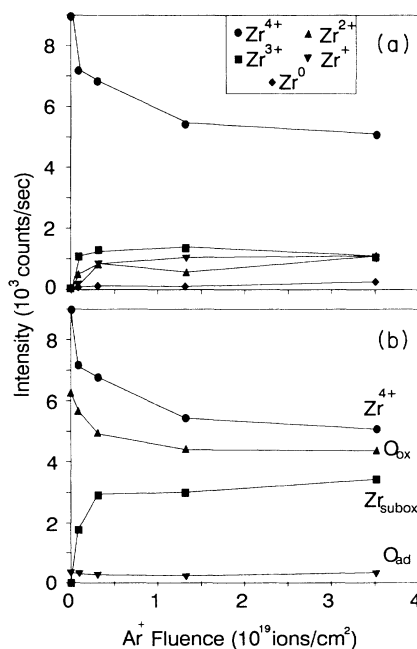


FIG. 2. (a) Intensities of the different contributions to the Zr $3d$ signal due to different oxidation states of zirconium: Zr^{4+} , Zr^{3+} , Zr^{2+} , Zr^+ , and Zr^0 , as a function of the Ar^+ fluence. (b) Intensities of the different contributions to Zr $3d$ (Zr^{4+} , $\sum_{n=0}^3 \text{Zr}^{n+}$) and O $1s$ (O_{ox} , O_{ad}) as a function of the Ar^+ fluence.

tensity decrease of the O 1s signal. The respective areas of the two components which conform the O 1s line have been depicted in Fig. 2(b) together with the intensities of the Zr⁴⁺ species and of the rest of the components of the Zr 3d signal considered as a whole and labeled as "subox" [cf. Fig. 2(a)]. Figure 2(b) shows that both the Zr⁴⁺ and O_{ox} decrease rapidly and almost parallel during Ar⁺ bombardment, whereas the signal associated with the reduced species increases. In addition, small amounts ($\sim \frac{1}{5}$ of a monolayer) of adsorbed oxygen appear to be present at the surface during the reduction process.

Zr 3d spectra were also measured at 30° with respect to the surface normal in order to make them more surface sensitive. These spectra (not shown) were also quantitatively analyzed and used to get more information about the distribution in depth of the different species. In fact, the ratio of intensities $I_{30^\circ}(\text{Zr}^{n+})/I_0(\text{Zr}^{n+})$ in the different oxidation states taken at 30° and 0° with respect to the surface normal is expected to increase when the corresponding species are enriched at the surface or the near-surface region. That ratio has been depicted in Fig. 3 as a function of the Ar⁺ fluence, but to simplify the analysis and to reduce the error introduced by the deconvolution procedure, intensities of Zr⁺ and Zr⁰ were considered together as well as those of Zr²⁺ and Zr³⁺.

Figure 3 suggests that the oxidation state of zirconium increases with depth. In fact, it is recognized that ZrO₂ lies in the substrate covered by a suboxide layer mainly formed by Zr³⁺ and Zr²⁺ on top of which Zr⁺ and Zr⁰ are present. A schematic representation of the assumed layer model showing the outermost monolayer, the altered layer, and the bulk has been drawn in Fig. 4. Although other models could be used, the choice which has been made appears reasonable and provides a clear insight into the observed compositional variations.

B. Thickness and composition of the altered layer

According to that model (cf. Fig. 4) of the altered layer a more quantitative insight into the composition and thickness can be realized in terms of the measured intensities.

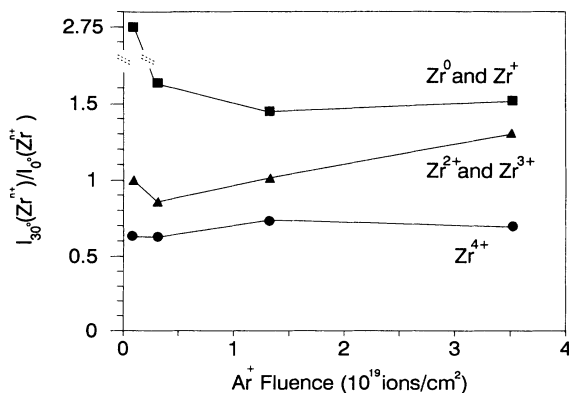


FIG. 3. Relative intensities of Zr 3d in the different oxidation states [Zr⁴⁺, (Zr³⁺ + Zr²⁺), (Zr⁺ + Zr⁰)], for 0° and 30° takeoff angles, as a function of the Ar⁺ fluence.

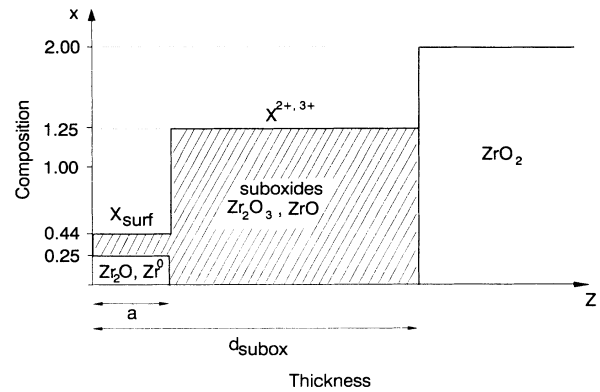


FIG. 4. Scheme of the altered layer induced by 3-keV Ar⁺ ions (z is the depth from the surface).

The intensities of Zr⁺ and Zr⁰ species account just for a fraction of the outermost monolayer, as can be easily obtained from

$$\frac{I(\text{Zr}^0)}{I^0(\text{Zr}^{4+})} \equiv \Theta_0 \frac{N_{\text{Zr}}^0}{N_{\text{Zr}}^4} [1 - \exp(-a/\lambda)] \quad (1)$$

and

$$\frac{I(\text{Zr}^+)}{I^0(\text{Zr}^{4+})} \equiv \Theta_1 \frac{N_{\text{Zr}}^1}{N_{\text{Zr}}^4} [1 - \exp(-a/\lambda)], \quad (2)$$

where $I(\text{Zr}^0)$ and $I(\text{Zr}^+)$ correspond to the intensities associated with Zr⁰ and Zr⁺ species, respectively, and $I^0(\text{Zr}^{4+})$ with the original (i.e., before sputtering) ZrO₂ sample. N_{Zr}^n is the atomic density of zirconium in the corresponding oxide ZrO _{$n/2$} and in pure metal (i.e., $n=0$) and a is the respective monolayer size estimated according to the expression

$$N_{\text{Zr}}^n = \frac{1}{a_{\text{Zr}}^3 + (n/2)a_{\text{O}}^3} = \frac{1}{a^3(1+n/2)}, \quad (3)$$

where a_{Zr} and a_{O} are the zirconium and oxygen atomic sizes as determined from the atomic densities in metallic zirconium and in ZrO₂ (i.e., 4.28 and 2.98×10^{22} atoms cm⁻³, respectively). The exponential factors in Eqs. (1) and (2) take into account the finite thickness a of the layer with respect to the inelastic mean free path λ of the photoelectrons.²¹ $\lambda = \lambda_{\text{Zr}} \approx \lambda_{\text{ZrO}_2} \approx 2$ nm was used in this work as estimated from the universal relation proposed by Seah and Dench.²²

The resulting $\Theta_0 + \Theta_1$ as a function of the Ar⁺ fluence has been depicted in Fig. 5. It shows that in the steady state the Zr⁰ and Zr⁺ species account for almost a monolayer, $\Theta_0 + \Theta_1 \approx 0.9$, with $\Theta_0 \approx 0.13$.

In addition, the equivalent thickness d_{subox} of the altered layer (supposed homogeneous) can be estimated in terms of the attenuation of the signal from the substrate [i.e., $I(\text{Zr}^{4+})$] as due to the overlayer of suboxides:

$$I(\text{Zr}^{4+}) = I^0(\text{Zr}^{4+}) \exp(-d_{\text{subox}}/\lambda). \quad (4)$$

The thickness calculated in this way has been

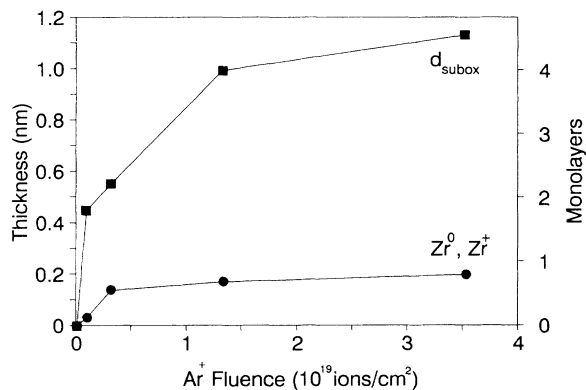


FIG. 5. Thickness of the outermost layer (Zr^0 , Zr^+) and of the whole altered layer (d_{subox}) as determined from Eqs. (1), (2), and (4) vs Ar^+ fluence. 1 monolayer $\equiv 0.24$ nm.

represented in Fig. 5, labeled as subox. Again, a rapid increase of d_{subox} up to fluences of about 1.5×10^{19} ions/cm² is observed to be followed by a region where the thickness appears to saturate at values close to $d_{\text{subox}} \sim 1.2$ nm.

The average composition ZrO_x of the two different layers in which the altered layer has been subdivided can also be estimated. Thus, considering that in the bombarded sample the outermost monolayer is formed by Zr^0 and Zr^+ species up to a fraction $\Theta \sim 0.9$ monolayers (ML's) and the rest $(1-\Theta)$ by Zr^{2+} and Zr^{3+} it results in an averaged composition x_{surf} given by

$$x_{\text{surf}} \equiv \Theta x(0,+) + (1-\Theta)x(2+,3+), \quad (5)$$

where

$$x(0,+) = \frac{1}{2} \frac{I(Zr^+)}{I(Zr^+) + I(Zr^0)} \quad (6)$$

and

$$x(2+,3+) = \frac{1}{2} \frac{2I(Zr^{2+}) + 2I(Zr^{3+})}{I(Zr^{2+}) + I(Zr^{3+})}. \quad (7)$$

Alternatively, the average composition \bar{x} of the whole altered layer was also estimated assuming a homogeneous distribution of the different suboxides, according to

$$\bar{x} = \frac{1}{2} \left[\frac{\sum_{n=0}^3 nI(Zr^{n+})}{\sum_{n=0}^3 I(Zr^{n+})} \right]. \quad (8)$$

The results of \bar{x} , $x(2+,3+)$, and x_{surf} as a function of the Ar^+ fluence have been depicted in Fig. 6. Obviously for an Ar^+ fluence equal to zero, $x_{\text{surf}} \equiv \bar{x} \equiv 2$ and $x(2+,3+) \equiv 0$. The values corresponding to the highest Ar^+ fluence (i.e., steady state) were used in the construction of the scheme shown in Fig. 4. It is worth mentioning that the surface layer appears more severely depleted in oxygen ($ZrO_{0.44}$) than the layer underneath ($ZrO_{1.3}$), which gives an altered layer 1.2 nm thick with an average composition ZrO in the steady state.

Since Ar^+ -induced reduction of oxides could depend on the method of preparation of the sample, an anodic

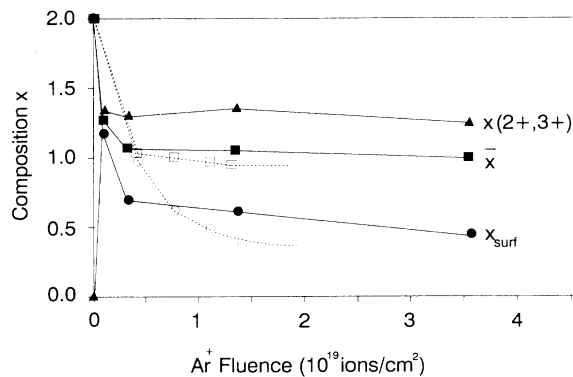


FIG. 6. Averaged compositions of the whole altered layer, \bar{x} , and of the two parts in which the altered layer has been subdivided, x_{surf} and $x(2+,3+)$, obtained from Eqs. (8), (5), and (7), respectively, vs Ar^+ fluence for a thermal (solid symbols) and anodic (open symbols) ZrO_2 .

ZrO_2 sample was also subjected to Ar^+ sputtering under the same conditions as for the thermal oxide. The results of \bar{x} and x_{surf} are also shown in Fig. 6 together with those corresponding to thermal ZrO_2 . Apart from divergences in the initial transient which is influenced by the contamination layer observed in anodic ZrO_2 , no significant differences were observed in the steady-state compositions \bar{x} of both oxides except for a slightly larger reduction in the outermost layer x_{surf} in the case of the anodic oxide. This difference could be related to a larger amount of defects and to the presence of the more easily reducible OH^- groups in the anodic oxide.

The above results show that 3-keV Ar^+ bombardment of ZrO_2 causes the formation of a variety of suboxide species which distribute inhomogeneously within the altered layer. In fact, it has been shown that the oxidation state of zirconium increases with depth, resulting in a surface monolayer severely depleted in oxygen (averaged composition $ZrO_{0.44}$) and three more monolayers with an averaged composition $ZrO_{1.2}$ (cf. Fig. 4). This structure is in good agreement with the idea of a bilayer model²³ where the atoms are sputtered from the surface, whereas the adjacent deeper layers are compositionally homogenized by Ar^+ -induced mixing and relocation processes. Therefore the lower oxidation states of zirconium generated at the outermost atom layer would be caused by preferential sputtering of oxygen. This would be in agreement with the large difference between the oxygen and zirconium surface binding energies estimated by Kelly² for ZrO_2 . According to his proposal,² that surface binding energy is the relevant factor for preferential sputtering of oxygen in ionic oxides.

Ar^+ bombardment of ZrO_2 appears to have been previously studied by Holm and Storp¹⁵ and Hofmann and Sanz,^{8,14} both groups using XPS. Holm and Storp¹⁵ reported a gradual chemical reduction of a series of very thin oxide films of different transition metals including ZrO_2 . However, the study is very qualitative. More recently, Hofmann and Sanz^{8,14} showed that anodic ZrO_2

undergoes reduction up to an averaged composition ZrO_{0.7} within an altered layer 1.3 nm thick when it is bombarded with 3-keV Ar⁺ ions. In general, their results are in good agreement with the results presented here. The difference in the averaged composition of the altered layer is mainly due to the gross quantification realized by Hofmann and Sanz^{8,14} in terms of just only two possible reduced states for zirconium (i.e., ZrO and metallic Zr) instead of the four considered here. In fact, the suboxide labeled as ZrO by Hofmann and Sanz^{8,14} at -1.6 eV with respect to the binding energy of ZrO₂ should be considered as a superposition of ZrO and Zr₂O₃, as labeled in this work, at -1.1 and -2.2 eV, respectively. Furthermore, the considerable amount of metallic Zr found by Hofmann and Sanz would be largely influenced by the presence of Zr₂O as observed here.

In fact, experimental spectra (cf. Fig. 1) do not show distinguishable features, which could be assigned to individual suboxides, but a continuous distribution with a small shoulder at the Zr₂O energy location. The oxide structure probably tends to adjust locally to different stable or metastable suboxides corresponding to the local composition produced by the combined effect of the surface preferential sputtering of oxygen and the induced atom diffusion and mixing. Within this picture, the signal attributed to Zr⁰ should not be considered as due to metallic Zr, but rather to elemental Zr, probably forming very small clusters, up to a total amount equivalent to 0.1 monolayer in the steady state.

C. Valence-band spectra

XPS was also used to monitor changes in the valence levels induced by Ar⁺ bombardment. Figure 7(a) shows valence-band spectra in the 0–40-eV binding energy range for the original ZrO₂ (bottommost curve) and after four different Ar⁺ fluences. MgK $\alpha_{3,4}$ satellites have been numerically subtracted. The corresponding spectrum for metallic zirconium has also been included for comparison (topmost curve). The spectra are dominated by the Zr 4p levels, but the O 2s and the molecular orbitals associated with the O 2p and Zr 4d valence levels can also be clearly observed. The Zr 4p levels in the oxide appear chemically shifted by ~ 4 eV to higher binding energy with respect to the metal.^{16,24}

The development of the ZrO₂ spectrum as the Ar⁺ fluence is increased in the amounts shown can be followed in Fig. 7(a). However, it is evident that those spectra correspond to contributions from both the altered layer and ZrO₂ in the substrate. Therefore we attempted to extract the contribution from the altered layer by subtracting the ZrO₂ contribution. The results are shown in Fig. 7(b), where an enlargement of the spectra near the Fermi level of ZrO_x (i.e., from the altered layer) after different Ar⁺ fluences is displayed together with those of Zr metal and ZrO₂.

The set of spectra assigned to the altered layer after different Ar⁺ fluences was obtained by subtracting a properly scaled spectrum of the valence band of ZrO₂. To find that scale factor for each spectrum, the contribution of the Zr⁴⁺ species to the Zr 3d XPS signal was

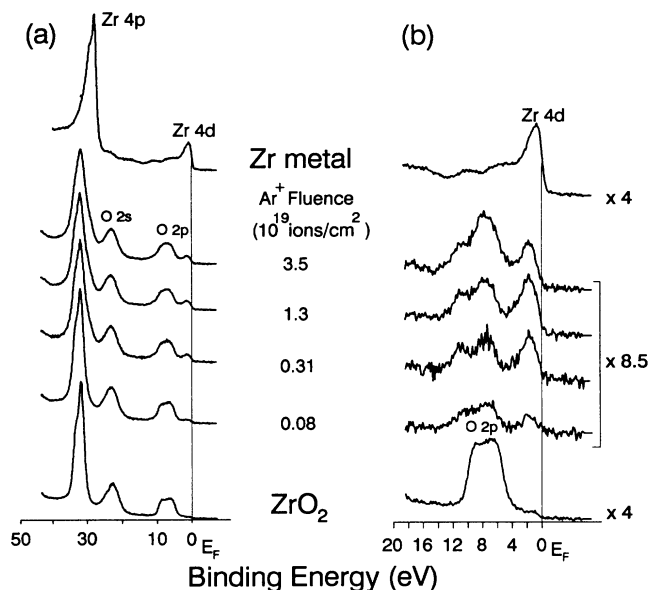


FIG. 7. XPS spectra of the valence band of Zr metal, ZrO₂, and ZrO₂ after bombardment with 3-keV Ar⁺ (fluence indicated in each spectrum). (a) Experimental spectra. (b) Spectra corresponding to the altered layer, obtained after subtraction of the ZrO₂ contribution as determined from the Zr 3d core levels (see text). The valence-band spectra of Zr and ZrO₂ are also included.

determined [cf. Fig. 2(a)] with respect to the intensity of the standard ZrO₂ [i.e., $C \equiv I(\text{Zr}^{4+})/I^0(\text{Zr}^{4+})$] and then corrected for the difference in inelastic mean free path by taking into account the respective kinetic energies of the Zr 3d and 4p levels. Thus the scale factor F for each spectrum was determined by

$$F = \exp \left[\frac{E_k^{1/2}(\text{Zr } 3d)}{E_k^{1/2}(\text{Zr } 4p)} \ln C \right] \quad (9)$$

according to a $\sim E_k^{1/2}$ dependence²² of the inelastic mean free path. In this way the contributions to the spectra of the Zr⁴⁺ species and the associated oxygen (i.e., ZrO₂) are supposedly suppressed.

Although the subtraction procedure must be understood as a rough estimate it provides a good method to isolate the valence-band structure of the altered layer. In fact, the subtracted spectra are representative of the altered layer as far as the assumed structure (cf. Fig. 4) is supported by the experimental data of Fig. 3.

Regarding the valence-band spectra of Fig. 7(b) significant differences can be observed with respect to that of ZrO₂. In the case of the original ZrO₂ the valence electrons are confined in the O 2p-derived band at energies between 4 and 10.6 eV as expected from a completely ionic model of Zr⁴⁺ and O²⁻ corresponding to a Zr 4d⁰ configuration. Reliable band calculations are presently not available because of its complex crystalline structure. In fact, to our knowledge, only a discrete-variational $X\alpha$ cluster calculation has been performed for tetragonal and cubic ZrO₂.²⁵ According to it the two small structures at

6.0 and 8.5 eV correspond to the O 2p σ and π molecular orbitals with a very weak d character, more significant on the high-binding-energy side of the band.²⁵

The top of the valence band at $E_B = 4.0$ eV agrees very well with an optical band gap of ~ 5 eV.²⁶ In addition, a weak emission in the gap extends from the top of the valence band up to the Fermi level, showing a maximum at $E_B \approx 1$ eV. It is usually ascribed to trapped electrons in oxygen vacancies and other surface defects.^{4-7,9-11} The signal height at the Fermi level yields a density of states (DOS) at the Fermi level (due to the defect states) of about 4% of that of Zr metal. Furthermore, the integrated intensity of the whole emission band in the gap corresponds to about 10% of the probed Zr atoms being in a Zr^{3+} state (i.e., 2.5% of oxygen vacancies), or in terms of electrons to an electron density of $\sim 3 \times 10^{21} \text{ cm}^{-3}$. Since the density of defect states is not uniform in the bulk but they probably concentrate at the near-surface region, the measured intensity could better be interpreted as an electron surface density of $0.6 \times 10^{15} \text{ cm}^{-2}$, i.e., approximately to a surface monolayer of oxygen vacancies. This high density of surface defects in ZrO_2 is caused by the preparation method (i.e., annealing at low oxygen pressures). In any case, the contribution of such a monolayer of Zr_2O_3 to the Zr 3d spectrum of the original ZrO_2 is very difficult to detect in the experimental data.

On the other hand, the spectra associated with the altered layer (i.e., ZrO_x) show a band emission in the energy range corresponding to O 2p in ZrO_2 with two clearly distinguishable features with a larger spin-orbit splitting and higher binding energy than in the original band of the ZrO_2 [cf. Fig. 7(b)]. Furthermore, a new broadband of emission appears in the band gap at ~ 2.3 eV above the top of the valence band of the oxide (i.e., $E_b \sim 1.7$ eV) which increases in intensity with Ar^+ fluence until saturation.

As mentioned above, such emission bands in the energy gap have usually been ascribed to trapped electrons in oxygen vacancies.^{4-7,9-11} However, at the high Ar^+ fluences used in this work the reduction and compositional changes of the altered layer are so significant that a simple model of oxygen vacancies in an otherwise ideal oxide structure cannot be considered. Rather, the modified oxide structure should be regarded as a highly defective one where the local zirconium-oxygen coordination corresponds to different suboxides, including oxygen vacancies and other defects. In fact, stoichiometric suboxides such as Ti_2O_3 and other transition-metal oxides^{5,27} show similar band emissions within the oxide band gap.

Alternatively, the subtraction of the valence-band spectrum of ZrO_2 from the spectra with the emission band in the gap [cf. Fig. 7(a)] can also be performed in terms of the respective intensities of the O 2s peaks instead of the Zr^{4+} 3d as above. In this case, the spectrum corresponding to ZrO_2 is subtracted until the O 2s signal is completely suppressed, neglecting the differences in inelastic mean free path along that energy range (0–30 eV). The results are plotted in Fig. 8 as dashed lines together with

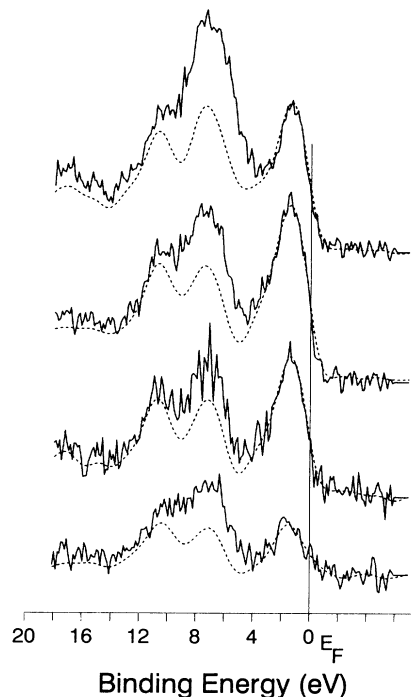


FIG. 8. Valence-band spectra of the altered layer (solid line) as given in Fig. 7(b) compared with the Zr 4d contributions (dashed line) resulting from the subtraction of the valence band of ZrO_2 until the O 2s signal is completely suppressed (see text for details).

the valence-band spectra of Fig. 7(b) (solid lines) for comparison. Surprisingly the signal in the region of the O 2p is not completely suppressed but a doublet structure remains together with the emission band in the gap, suggesting that the observed signal between 4 and 12 eV [cf. Fig. 7(b)] cannot be completely assigned to oxygen as in ZrO_2 .

Assuming that the O 2p partial density of states of the ZrO_x suboxides is similar to that of ZrO_2 , then these spectra (dashed curves) in Fig. 8 roughly represent the Zr 4d covalent admixture to the molecular orbitals of ZrO_x . This contribution dominates the valence-band spectra due to its higher photoemission cross section, as can be estimated, from the spectra of ZrO_2 and Zr metal in Fig. 7(a):

$$\frac{\sigma(Zr\ 4d^1)}{\sigma(O\ 2p^1)} = \frac{[I(VB)/I(Zr\ 4p)]_{Zr_m}/2}{[I(VB)/I(Zr\ 4p)]_{ZrO_2}/12} = 6.3, \quad (10)$$

where $\sigma(Zr\ 4d^1)$ and $\sigma(O\ 2p^1)$ are the respective photoemission cross sections per electron, $I(VB)$ is the intensity of the corresponding valence band, and the numerical factors (i.e., 2 and 12) take into account the corresponding electronic populations per Zr atom assuming pure ionic bonding in ZrO_2 . The result is in reasonable agreement with the estimated value (7.9) in terms Scofield's theoretical values.²⁸ The difference is within the expected deviations of the calculated σ data and could also be explained by just a small ($\sim 4\%$) covalent admixture of Zr 4d levels.

This interpretation of the dashed spectra in Fig. 8 can be supported by observing their correlation with the intensity of the Zr 3d signal associated with the suboxides. This is shown in Fig. 9, where the intensity of the whole Zr 4d spectra represented as dashed curves in Fig. 8 (solid squares) and the partial intensity of the emission band in the gap at $E_B = 1.7$ eV (open squares) have been plotted as a function of the Zr 3d intensity of the suboxides (i.e., $Zr^{3+} + Zr^{2+} + Zr^{+} + Zr^0$) and compared with the corresponding values of Zr metal (solid circle) and of the original ZrO₂ (open triangle). The figure clearly shows that, whereas in the first case, i.e., assuming that the whole dashed spectra correspond to the Zr 4d, the correlation with the intensity of the suboxide species is good and tends adequately to the value of the metal, in the second case, where only the emission band in the gap is considered, only 62% ($\pm 3\%$) of the Zr 4d states in the metal could be accounted for by linear extrapolation.

Taking into account the relative photoemission cross section, the overall Zr 4d contribution to the valence band can be estimated as 26%, ranging from 100% in the case of the band in the gap just below E_F , to only $\sim 16\%$ in average in the region of the O 2p orbitals.

The height of the valence band at E_F , that is proportional to the DOS at Fermi level, can also be measured and compared with the value of Zr metal using the suboxide Zr 3d intensity as normalization. The results follow the same behavior as the integrated intensity of the defect or suboxide band at $E_B = 1.7$ eV (cf. Fig. 9) tending to 56% ($\pm 3\%$) of the metal value, which represents $\sim 45\%$ of the DOS (per unit volume) of the Zr metal if an atomic density of the suboxide $N_{Zr}^{ZrO} \sim 0.8N_{Zr}^{metal}$ is assumed.

Another interesting question refers to the observation of band bending as a consequence of the reduction of the surface. In fact, it is well established that electrons trapped in oxygen vacancies of transition-metal oxides occupy localized levels originating from the lower empty

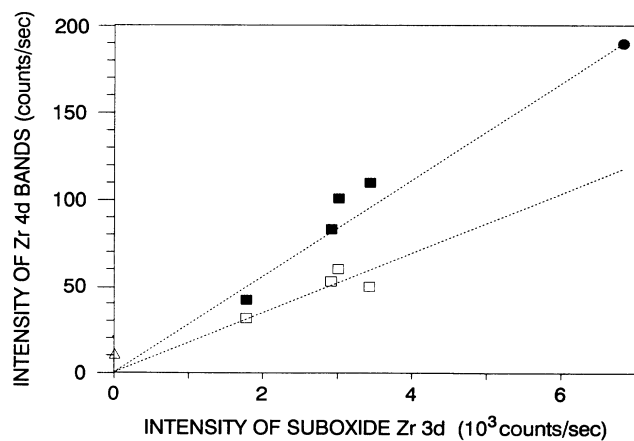


FIG. 9. Intensity of the Zr 4d bands (dashed curves in Fig. 8) as a function of the intensity of the Zr 3d signal associated with the suboxides. Whole Zr 4d band, solid squares. Band just below E_F , open squares. Values for Zr metal (triangle) and ZrO₂ (circle) are also included.

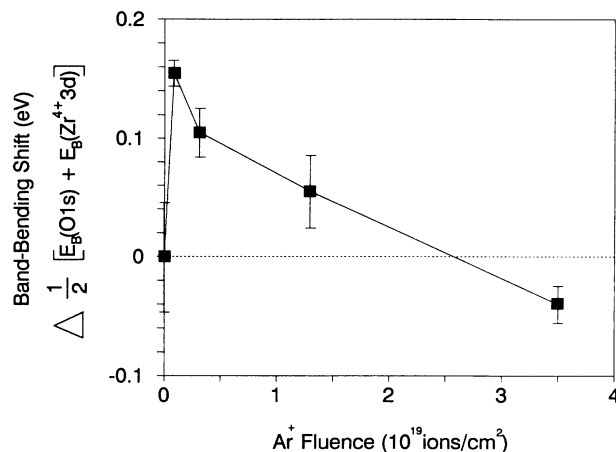


FIG. 10. Binding energy of the midpoint between the O 1s and Zr⁴⁺ 3d XPS lines relative to that corresponding to the original ZrO₂ sample as a function of the Ar⁺ fluence. Error bars indicate the deviations of the difference in binding energy [$E_B(O\ 1s) - E_B(Zr^{4+}\ 3d)$] from the average value of 347.93 eV.

orbitals of the cations, which push up the Fermi level and cause bending of the whole electronic structure to higher binding energies.²⁷ In our case, the shift produced by ion bombardment is expected to be very small since the ZrO₂ sample is already of *n* type due to its high density of surface point defects. However, in order to detect a possible band bending shift we have represented in Fig. 10 the parallel shift of the Zr and O core levels, defined in terms of their respective binding energies as $\frac{1}{2}[E_B(O\ 1s) + E_B(Zr^{4+}\ 3d)]$ versus the Ar⁺ fluence. The error bars indicate the deviations of the energy difference [$E_B(O\ 1s) - E_B(Zr^{4+}\ 3d)$] from its average value of 347.93 eV. The figure shows that for the smallest Ar⁺ fluence, a small shift of about 0.2 eV can be detected; however, this shift decreases as the Ar⁺ fluence is increased because of the screening effect of the altered layer, which becomes more reduced (cf. Figs. 5 and 6). It indicates again that for the ion fluences used in this work we are not in a well-defined state of surface point defects and oxygen vacancies, but in an ill-defined altered layer formed by different suboxides.

IV. CONCLUSIONS

It has been shown that 3-keV Ar⁺ bombardment of ZrO₂ leads to significant compositional changes and the buildup of an altered layer ~ 1.2 nm thick. This layer is characterized by an important oxygen depletion, which causes the reduction of the original Zr⁴⁺ species to lower oxidation states. In terms of the intensities of the XPS core levels the altered layer has been quantitatively characterized and the in-depth distribution of the different oxide phases was determined. It is shown that the altered layer (1.2 nm thick, averaged composition ZrO) consists in a surface monolayer severely depleted in oxygen (averaged composition ZrO_{0.44}) and four more

monolayers with an averaged composition $ZrO_{1.2}$.

Ar^+ bombardment of ZrO_2 results also in drastic changes of the valence band. By comparing the intensities of the corresponding core levels and valence-band signals, the electronic structure of the reduced surface (ZrO_x) could be determined. It is shown that the valence band of the altered layer shows two clearly distinguishable structures in the energy range of the O 2p band, as well as a band emission at 2.3 eV above the top of the valence band. They are clearly associated with compositional changes, $ZrO_2 \rightarrow ZrO_x$, according to a highly oxygen deficient random distribution of different zirconium-

oxygen coordinations caused by Ar^+ bombardment. In addition, the Zr 4d contribution to the valence band of the altered layer could also be estimated, showing that it accounts for the whole emission in the band gap and very significantly for the emission in the energy range of the O 2p band.

ACKNOWLEDGMENTS

This research was financially supported by the CICYT of Spain through Contract Nos. Mat 513/90 and ESP-89-0182.

- ¹G. Betz and G. K. Wehner, in *Sputtering by Particle Bombardment II*, edited by R. Behrish (Springer, Berlin, 1984), Chap. 2.
- ²R. Kelly, in *Beam Modification of Materials, Ion Beam Modification of Insulators*, edited by P. Mazzoldi and G. W. Arnold (Elsevier, Amsterdam, 1987) Chap. 2, and references therein.
- ³V. E. Henrich, G. Dresselhaus, and H. J. Zeiger, *Phys. Rev. B* **17**, 4908 (1978).
- ⁴V. E. Henrich and R. L. Kurtz, *Phys. Rev. B* **23**, 6280 (1981).
- ⁵R. L. Kurtz and V. E. Henrich, *Phys. Rev. B* **25**, 3563 (1982).
- ⁶F. Werfel and E. Minni, *J. Phys. C* **16**, 6091 (1983).
- ⁷W. Göpel, J. A. Anderson, D. Frankel, M. Jaehnig, K. Phillips, J. A. Schäfer, and G. Rucker, *Surf. Sci.* **139**, 333 (1984).
- ⁸S. Hofmann and J. M. Sanz, *J. Trace Microprobe Tech.* **1**, 213 (1982).
- ⁹R. Courths, P. Steiner, H. Höchst, and S. Hüfner, *Appl. Phys.* **21**, 345 (1980).
- ¹⁰K. E. Smith and V. E. Henrich, *Solid State Commun.* **68**, 29 (1988).
- ¹¹R. Courths, B. Cord, and H. Saalfeld, *Solid State Commun.* **70**, 1047 (1989).
- ¹²A. R. Gonzalez-Elipse, G. Munuera, J. P. Espinos, and J. M. Sanz, *Surf. Sci.* **220**, 368 (1989).
- ¹³H. H. Kung, *Transition Metal Oxides: Surface Chemistry and Catalysis* (Elsevier, Amsterdam, 1989).
- ¹⁴S. Hofmann and J. M. Sanz, *Microchim. Acta Suppl.* **10**, 135 (1983).
- ¹⁵R. Holm and S. Storp, *Appl. Phys.* **12**, 101 (1977).
- ¹⁶C. Morant, J. M. Sanz, L. Galán, L. Soriano, and F. Rueda, *Surf. Sci.* **218**, 331 (1989).
- ¹⁷A. Savitzky and M. J. E. Golay, *Anal. Chem.* **36**, 1627 (1964).
- ¹⁸A. Proctor and P. M. A. Sherwood, *Anal. Chem.* **52**, 2315 (1980).
- ¹⁹D. A. Shirley, *Phys. Rev. B* **5**, 4709 (1972).
- ²⁰H. E. Bishop, *Surf. Interface Anal.* **3**, 272 (1981).
- ²¹M. P. Seah, in *Practical Surface Analysis Vol. 1—Auger and X-ray Photoelectron Spectroscopy*, edited by D. Briggs and M. P. Seah (Wiley, New York, 1990), Chap. 5.
- ²²M. P. Seah and W. A. Dench, *Surf. Interface Anal.* **1**, 2 (1972).
- ²³G. Carter, I. V. Katardjiev, and M. J. Nobes, *Surf. Interface Anal.* **14**, 194 (1989).
- ²⁴C. Palacio, J. M. Sanz, and J. M. Martinez Duart, *Surf. Sci.* **191**, 385 (1987).
- ²⁵M. Morinaga, H. Adachi, and M. Tsukada, *J. Phys. Chem. Solids* **44**, 301 (1983).
- ²⁶P. Meisterjahn, H. W. Hoppe, J. W. Schultze, *J. Electroanal. Chem.* **17**, 159 (1987).
- ²⁷V. E. Henrich, in *Surface and near-Surface Chemistry of Oxide Materials*, edited by J. Nowotny and L. C. Dufour (Elsevier, New York, 1988), Chap. 2.
- ²⁸J. H. Scofield, *J. Electron Spectrosc. Relat. Phenom.* **8**, 129 (1976).